Intensive Structural Disorder Induces Electronic Delocalization: Amorphous Solid-Liquid Transition in Ovonic Threshold Switching Materials

Nian-Ke Chen, Bai-Qian Wang, Meng Niu, Hong-Bo Sun, Shengbai Zhang, and Xian-Bin Li*

Disorder-induced electronic localization is responsible for the OFF state of the Ovonic threshold switching (OTS) device, which is an indispensable component in the present 3D-crossbar-architecture phase-change memory circuit. However, the atomic mechanism of the OTS device, especially the role of thermal effect, remains a long-term open question. Recent researches suggest that the working current of the OTS ON-state is often large enough to melt the adjacent phase-change memory material in the OTS+PCM devices. Thus, Joule heating-induced atomic/electronic structure transition in OTS materials must be seriously considered. Taking the typical OTS material GeSe as an example, first-principles calculations reveal an unexpected electronic delocalization induced by the enhanced structural disorder upon solid-liquid transition. Meanwhile, as the temperature rises, the band gap decreases or even closes, leading to an increase in carrier concentration. Therefore, the melting filament with high conductivity could be responsible for the holding-ON state of OTS materials. The results in this study may provide possible explanations for some puzzles of OTS devices, such as the reasons for holding-ON state and limited endurance.

1. Introduction

The electronic conductivity of amorphous materials is often very low due to the localized electronic states in disordered systems.[1]

N.-K. Chen, B.-Q. Wang, M. Niu, X.-B. Li
State Key Laboratory of Integrated Optoelectronics
College of Electronic Science and Engineering
Jilin University
Changchun 130012, China
E-mail: lixianbin@jlu.edu.cn
H.-B. Sun
State Key Laboratory of Precision Measurement Technology and Instruments
Department of Precision Instrument
Tsinghua University
Beijing 100084, China
S. Zhang
Department of Physics
Applied Physics, and Astronomy
Rensselaer Polytechnic Institute
Troy, NY 12180, USA

Utilizing insulating properties of amorphous semiconductors, Ovshinsky invented the Ovonic threshold switching (OTS) device where amorphous materials ensure an OFF state at their ground state but can be switched to the ON state after a threshold voltage is applied.[2] Recently, the OTS device, called the selector, has become a key component in the high-density memory integrated circuits based on 3D crossbar technology, such as phase-change memory (PCM) and resistive memory.[3]

Despite the diversity of previously proposed mechanisms,[4–15] it is generally believed that OTS is electronic-initiated with more or less thermal-assisted carrier excitation.[11,16] Also, some electronic models regard that atomic structures of OTS materials remain basically unchanged upon switching. However, in the real 3D-crossbar device unit built by OTS and PCM cells in series (OTS+PCM), the RESET voltage is often larger than the threshold voltage (V_{th}) to ensure that the current density of RESET operation is large enough to melt the PCM cell.[17] As a result, the Joule heating effect can be significant, which will lead to structural changes in OTS materials. In other words, even though the switching is electronically initiated, the subsequent Joule heating effect should be notable in the holding-ON state. Therefore, the effect of thermal heating on atomic/electronic structure transitions in OTS materials of the OTS+PCM structure, which is often omitted in previous investigations, must be carefully considered.

In this work, to clarify the influence of thermal heating, the atomic/electronic structure transitions of a typical OTS material (non-crystalline GeSe) under varied temperatures from 300 to 1500 K are investigated by first-principles calculations. As the temperature increases, more structural and chemical disorders emerge, such as deviated bond lengths, distorted bond angles, and increased wrong bonds. The enhanced disorder leads to a band shifting, and thereby narrows or even eliminates the band gap of the OTS material. That helps to produce considerable thermal-activated carriers. Unexpectedly, when amorphous GeSe (*a*-GeSe) melts into liquid GeSe (*l*-GeSe), the electronic localization of band-tail states dramatically decreases despite increasing structural and chemical disorders. Therefore, a mechanism of structural Disorder Induced electronic Delocalization (DID) is

**ADVANCED
SCIENCE NEWS**

www.advancedsciencenews.com

**ADVANCED
FUNCTIONAL
MATERIALS**

www.afm-journal.de

proposed. Here, both the delocalized electronic states and the increased concentration of carriers should significantly enhance the conductivity of GeSe, which explains well the holding-on state of the OTS process in real devices. The proposed DID mechanism should play a significant role in the OTS+PCM devices. The present study offers a new picture of the OTS working process, which provides references for the material design and corresponding thermal management. We suggest the melting of OTS materials should be taken into account carefully, especially in the OTS+PCM devices of 3D crossbar memory technology.

2. Results and Discussion

2.1. Atomic Structures during Amorphous Solid-Liquid Transition

Before the first-principles simulations, we approximately estimate the Joule heating effect in an OTS+PCM nanodevice using the finite-element analysis. The method has been used to study OTS and OTS+PCM devices.[17] We mainly compare the temperatures of OTS and PCM cells in the OTS+PCM device when the electrical current is large enough to RESET the PCM cell, i.e., melt the crystalline $Ge_2Sb_2Te_5$ (see Note S1, Supporting Information for more details). To simplify, we simulate Joule heating and thermal diffusion effects of the PCM+OTS cells in series under a rectangle electrical pulse to mimic the holding-ON state with a steady holding current (Figure S1a,b, Supporting Information). To meet the requirements for melting the PCM materials, we selected an input voltage that can heat the PCM cell to ≈1000 K, exceeding the melting point of the PCM materials (≈900 K for $Ge_2Sb_2Te_5$). At the same time, we examine the temperature of the OTS cell that is in series with the PCM cell (Figure S1c,d, Supporting Information). In the results, the highest temperature of the OTS cell can reach 1260 K, which is higher than the melting point of crystalline GeSe (≈960 K). Furthermore, if a confined conducting filament covering a partial region within the OTS cell is considered, the thermal effect will be more pronounced due to the increased current density (see Note S1 and Figure S2, Supporting Information). Therefore, thermally induced atomic/electronic structure transitions of OTS materials should have substantial effects on OTS+PCM nanodevices. It deserves a further detailed investigation.

Next, we investigate the structural evolution of disordered GeSe from room temperature to high temperature by ab initio molecular dynamic (AIMD) simulations (see Method for more details). **Figure 1a** shows the atomic mean square displacements (MSD). Below 700 K, the MSDs are quite small suggesting the stable states of a-GeSe at relatively low temperatures. Above 1100 K, a linear increase of MSD with time indicates forming liquid states with significant atomic diffusions. The inset in Figure 1a displays a transient structure of l-GeSe at 1500 K. Figure 1b,c show the bond angle distribution (BAD) around Ge and Se atoms, respectively. At 300 K, the main peak of the BAD is located at 90°, which stems from defective octahedral motifs. As a kind of typical defective octahedral motifs, pyramidal configurations are highlighted in Figure S3a,b (Supporting Information). Such configurations reveal a general p-bonding feature in a-GeSe. In fact, amorphous structure does not mean a complete disorder but has a specific short-range order due to rules of chemical bonding, such as the 8-N rule and the theory of orbital hybridization.

However, the local p-bonding configuration of GeSe will gradually deviate from its stable state when temperature increases. As such, the BADs centering at ≈90° gradually become broader and the new BADs at ≈50–60° appear, suggesting a breaking of the original short-range orders. This is because new triangle atomic motifs are formed in the liquid state (Figure S3c, Supporting Information). The pair correlation functions (PCF) in Figure 1d–f have a consistent trend, i.e., as the temperature rises, the peak of normal bonds (Ge-Se) becomes broader and lower while the peaks of the wrong bonds (Ge-Ge and Se-Se, < 3 Å) gradually appear. The next-nearest peaks of PCF for Ge-Ge pairs (close to 4 Å) are eliminated after melting, indicating that the mid-range order is lost. In brief, the structural and chemical disorder is strongly enhanced by thermal melting in GeSe.

### 2.2. Electronic Properties during Amorphous Solid-Liquid Transition

Next, we make efforts to clarify how the strong disorder in OTS materials in melting states can influence their electronic property and conductivity. **Figure 2a–e** show the density of states (DOS) of a-GeSe and l-GeSe. Here, the electronic properties are analyzed using transient structures in the equilibrium MD simulations at various temperatures (see Note S2 and Figure S4, Supporting Information). Both the valence band and conduction band are mainly composed of p orbitals, which corresponds with the existence of defective octahedral configurations. The electronic states involved in chemical bonding are also evaluated by the crystal orbital Hamilton population (COHP) analysis (Figure S5, Supporting Information). Please note that the states close to the top part of the filled band at around Fermi level (E_f) are composed of anti-bonding states,[18] which are mainly contributed by Ge-Se middle/long bonds no matter at room-temperature 300 K or high-temperature 1500 K.

At 300 K, a band gap of a-GeSe can be clearly observed despite existing defect states near the gap, see Figure 2a. Generally, such defect states are located at band edges in the form of Urbach tails.[19] As the temperature increases, the band gap gradually decreases, and completely disappears when the temperature exceeds 1100 K (Figure 2b–e). Moreover, the states near the Fermi level of l-GeSe continuously increase as the temperature rises. This is related to the enhancement of structural and chemical disorders by the temperature increase. Next, thermally activated carriers can be approximately estimated according to the total DOS evolution and the Fermi-Dirac distributions by the following two equations,[20]

$$N_e = \int_{E_f}^{+\infty} DOS \cdot f_{FD}(E, T) \ dE \tag{1}$$

$$N_h = \int_{-\infty}^{E_f} DOS \cdot [1 - f_{FD}(E, T)] \ dE \tag{2}$$

where E is the relative energy, T is the temperature, N_e is the number of electrons in the conduction band, N_h is the number of holes in the valence band, DOS is the total density of states, and f_{FD} is the Fermi-Dirac distribution function. The total concentrations of carriers ($N_e + N_h$) are shown in Figure 2f. At $T >$
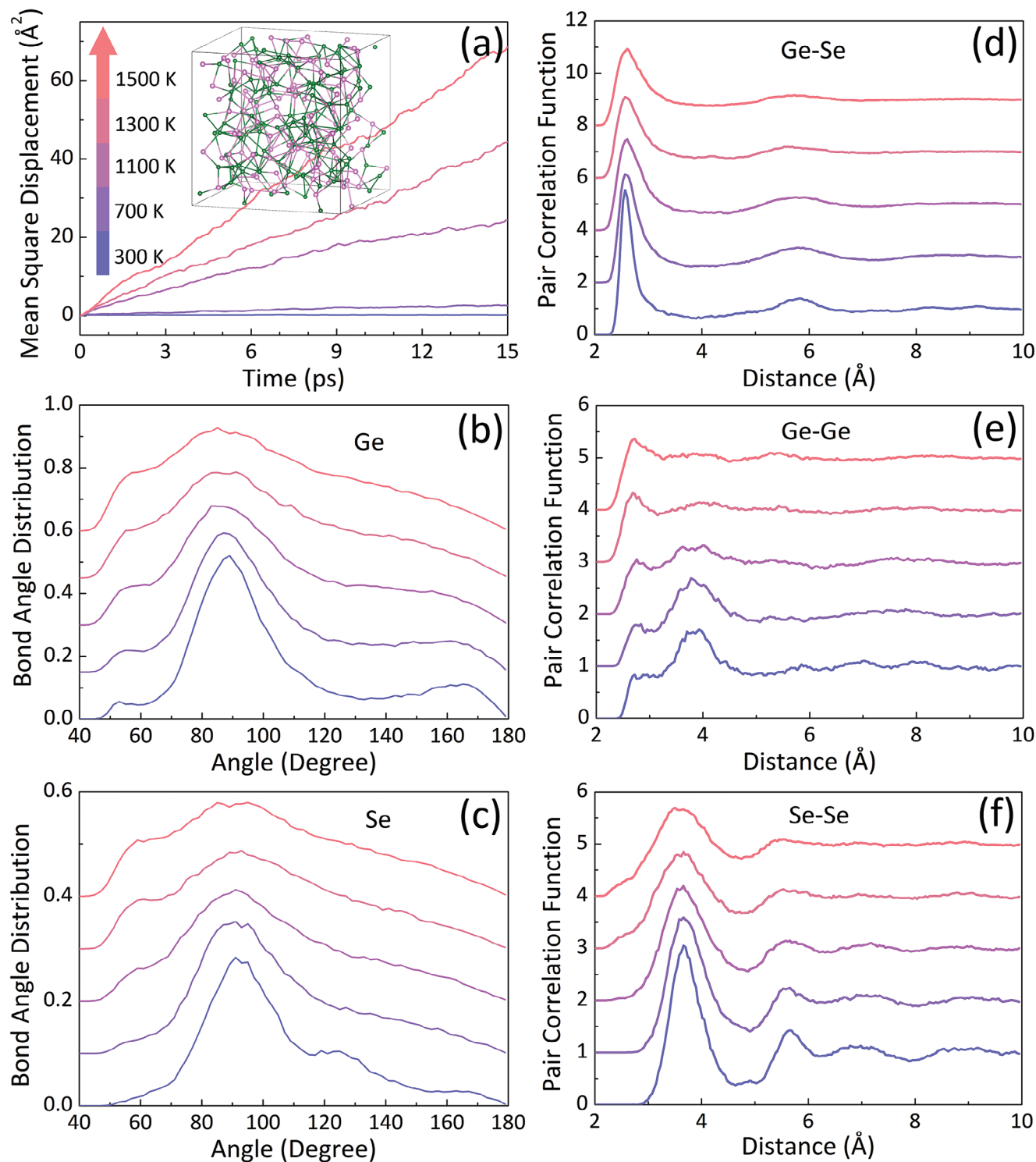
Figure 1. Disordered structures of GeSe at temperatures of 300, 700 K (for *a*-GeSe), and 1100, 1300, 1500 K (for *l*-GeSe). a) Mean square displacement (MSD) of atoms. b and c) Bond angle distribution (BAD) around Ge and Se atoms, respectively. d–f) Pair correlation function (PCF) of Ge-Se, Ge-Ge, and Se-Se atoms, respectively. The inset of the color bar in a) reflects the evolution of temperatures and is also applied to b–f). A snapshot of *l*-GeSe at 1500 K is also shown in the inset of a) where the green and pink balls represent Ge and Se atoms, respectively.
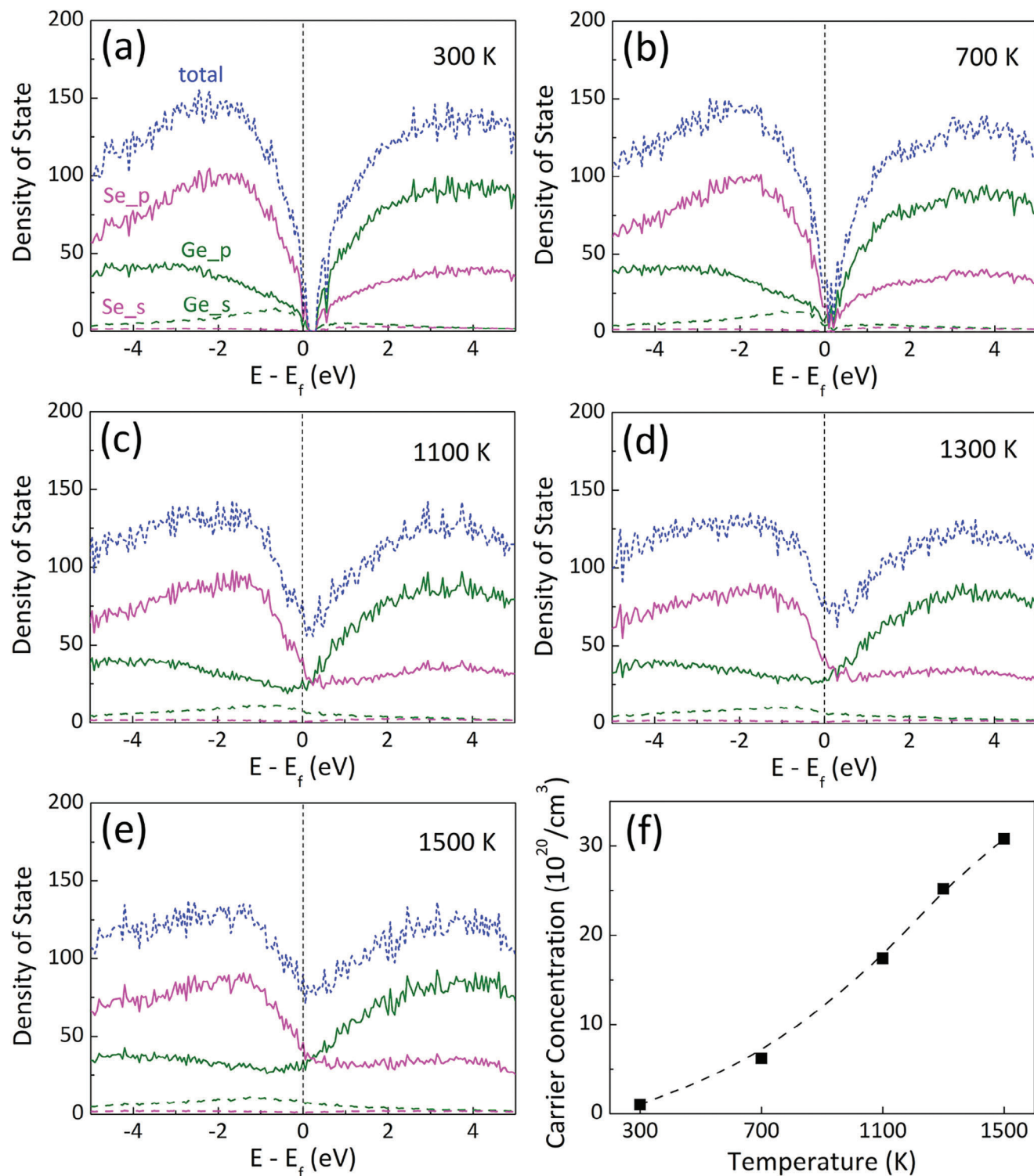
Figure 2. Total and partial DOS of *a*-GeSe at a) 300 K, b) 700 K, and *l*-GeSe at c) 1100 K, d) 1300 K, e) 1500 K. f) Estimated carrier concentrations of GeSe at various temperatures.
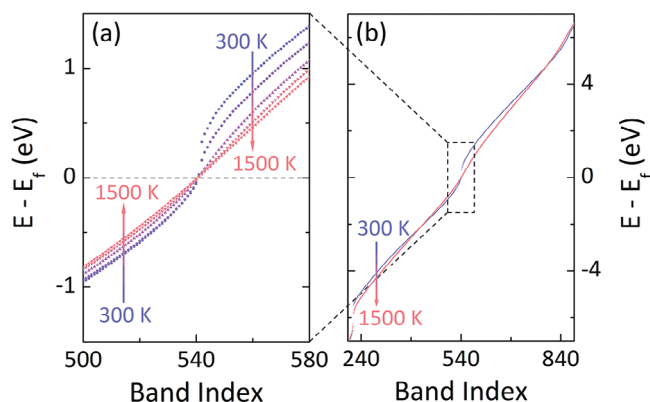
Figure 3. Band-decomposed energy distribution of a-GeSe and l-GeSe at the range of a) [−1.5, 1.5] eV and b) [−7, 7] eV. Each point represents an energy level. The arrows indicate the direction of the band shifting as the temperature rises.

1100 K of liquid states, the carrier concentration significantly increases by more than an order of magnitude compared to that at room temperature of a-GeSe. This offers proof of conductive characteristics in l-GeSe.

A further understanding of the band gap closing in Figure 2 is critical to clarify the structure-property correlation in GeSe amorphous and liquid states. In fact, the narrowing of band gap induced by temperature elevation has been reported in other amorphous chalcogenide semiconductors, such as $Ag_4In_3Sb_{67}Te_{26}$, $Ge_2Sb_2Te_5$, GeTe, As_2S_3, As_2Se_3, $GeSe_2$, Se and so on.[21–23] The mechanism has been attributed to band broadening by lattice vibrations or band shifting by electron-lattice interactions.[23] Here, to further explore the origin of the change of electronic structure in Figure 2, the band-decomposed energy distributions of a-GeSe and l-GeSe at various temperatures are calculated. **Figure 3a** shows the energy levels close to Fermi level, i.e., [−1.5, 1.5] eV. Clearly, the band-gap closing is caused by the shifting of the valence and conduction bands. No matter in the amorphous or liquid state, the tendencies are the same, i.e. (at around E_f) the energy levels above E_f would drop down while the ones below E_f would lift up as the temperature increases, accompanying the enhanced structure disorder. However, when checking a larger energy range, such as [−7, 7] eV, the direction of band shifting in [−5, −2] eV (see the arrow in Figure 3b) opposites to that in [−2, 0] eV close to E_f. In other words, temperature elevation does not lead to a uniform shifting up of the valence band but makes valance band distribution broader. The band shifting in Figure 3a can be regarded as a result of the change of lattice potential as the temperature rises.

2.3. Disorder-Induced Electronic Delocalization in Liquid OTS Materials

Although the concentration of carriers can be increased by melting (see Figure 2f), generally structural disorder may induce electronic state localization and would not benefit a high mobility of carriers.[1] Therefore, one may wonder whether such a "metallic"-like DOS in the liquid state (see Figure 2c–e) can contribute an effective conductance. To answer the question, the electronic localization degrees of the bands near the Fermi level are analyzed.
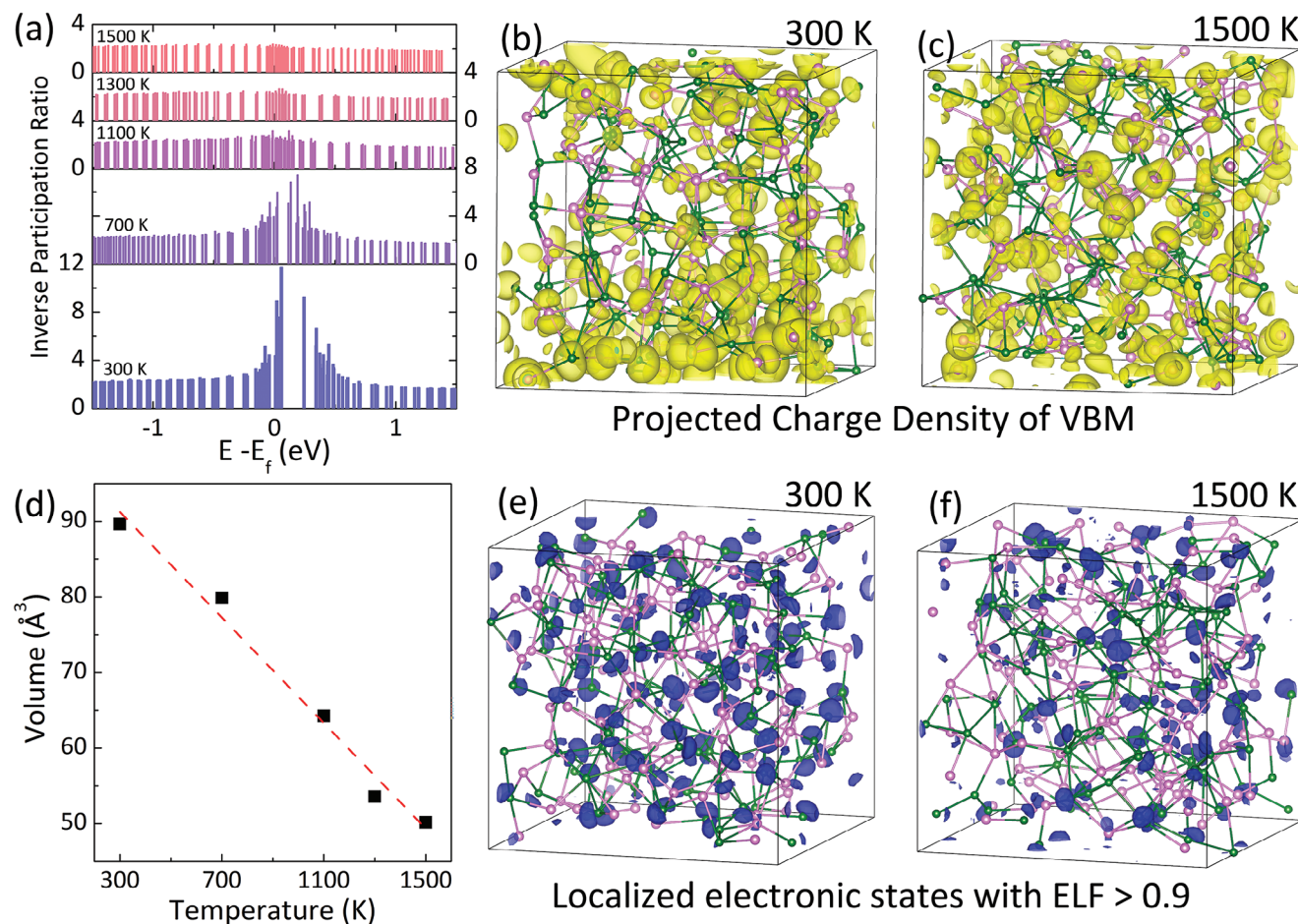
The localization of an orbital in real space can be estimated by inverse participation ratio (IPR), $I(\psi_n)$[24]

$$I\left(\psi_n\right) = N\frac{\sum_{i=1}^{N}\left|\psi_n\left(\vec{r}_i\right)\right|^4}{\left|\sum_{i=1}^{N}\left|\psi_n\left(\vec{r}_i\right)\right|^2\right|^2} \tag{3}$$

where N is the number of the sampled volume elements and i indicates their index. Within such a definition, a large IPR indicates a *localized* real-space distribution of ψ_n while a small IPR indicates a *delocalized* distribution. **Figure 4a** shows the calculated IPR at various temperatures. At 300 K, the IPRs of the band-edge states are obviously larger, suggesting they are localized. This agrees with the existence of Urbach tails or localized electronic states near band edges in OTS materials at room temperature. When the temperature increases, the IPRs of localized band tails gradually decrease. In particular, when the material is melted, the band tails or localized states almost disappear and those around E_f are also changed to extending states. In other words, after melting the disorder-induced states in fact become delocalized. Note that the present phenomena of gap closing and electronic delocalization in GeSe revealed by the PBE functional are also confirmed by the higher-level hybrid functional of HSE06 (see Note S3 and Figure S6, Supporting Information).

Figure 4b,c show the projected charge density of the valence band maximum (VBM), which indeed becomes more extended when the temperature increases from 300 to 1500 K. To further check the electronic localization of the system, the electron localization function (ELF)[25] is calculated. Figure 4d shows the volume of the highly localized states with the ELF value > 0.9. The volume of the highly localized states is found to decrease linearly with increasing temperature. Figure 4e,f show the spatial distribution of these states (ELF > 0.9). The decrease of the highly localized states can be clearly seen from 300 to 1500 K. This is consistent with the IPR analyses. Note that, the important conclusions including the intensive disorder-induced electronic delocalization and the closing of band gaps after the solid-to-liquid transition can be also applied in another typical OTS material of $GeSe_2$ with a larger band gap (see Figures S7 and S8, Supporting Information). That may suggest a relative generality of these conclusions in OTS materials.
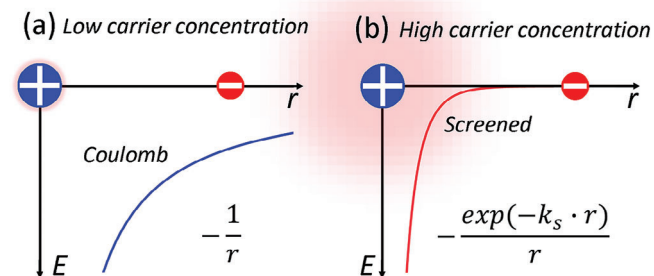
The change in the electronic localization degree of OTS materials after melting can be understood by a phenomenological picture. At room temperatures, the electrons in band tails are trapped in defects or local atomic environments. When the temperature increases above the glass transition temperature, atoms begin to significantly relax and change their surrounding structures. Especially, when the material is melted, electronic delocalization will happen. As a result, the electrons originally trapped in the defects, or the local atomic environment can be de-trapped. In brief, at room temperature, a-GeSe is an insulator because the carrier concentration is low, and the band-edge/defect states are localized. As the temperature increases, the band gap decreases, leading to a higher concentration of thermally excited carriers. The mobility of these carriers is also enhanced due to the extended electronic wavefunction according to the IPR analysis (Figure 4a). Furthermore, based on the fact that high-concentration carriers can help to screen the Coulomb

**ADVANCED
SCIENCE NEWS**

www.advancedsciencenews.com

**ADVANCED
FUNCTIONAL
MATERIALS**

www.afm-journal.de

Figure 4. Electronic localization degrees of *a*-GeSe and *l*-GeSe at varied temperatures. a) Energy level-decomposed inverse participation ratio (IPR). b and c) Projected charge density of the VBM. The value of the isosurface is 0.0002 e/a_0^3, a_0 is the Bohr radius. d) The volume of the highly localized states with electron localization function (ELF) > 0.9. e) and f) The spatial distribution of the highly localized states with ELF > 0.9 at 300 K and 1500 K, respectively. The color used in a) follows the color bar in Figure 1a, indicating the change of IPR from 300 K (bottom column) to 1500 K (top column).

interaction between carriers and ions (**Figure 5a,b**),[26] the carrier scattering from disordered ions in liquid could be reduced. In summary, when the OTS material is melted, it should behave like a conducting metallic state, thereby facilitating the maintenance of the ON-state in OTS materials. In fact, some experiments have

indeed observed low resistance states in the melted chalcogenide materials, such as GeAsTe and GeSbSe.[27,28] Recently, in situ experimental observations also found that the switching of a Te-element OTS material is accompanied by a phase transition from the crystalline phase to its liquid phase, which is considered a low-resistance state.[29]

2.4. Discussion on OTS Mechanism

We discuss the role of the Joule heating-induced structural transitions in applications of OTS+PCM devices. As mentioned before, the ON-state current should be large enough to melt the PCM cell. As such, the melting of OTS materials would be probable because OTS and PCM materials usually exhibit similar liquid-phase temperature ranges.[30,31] Then, this thermally induced transition benefits a significant enhancement of conductivity in OTS materials.

Moreover, it was reported that the holding voltage (V_h) of the OTS process is independent of the thickness of the OTS material, strongly indicating that the voltage drop mainly

Figure 5. Schematics of a) weak and b) strong screening effect (by carriers) between electron and ion to mimic the cases in amorphous and liquid OTS materials, respectively. $1/k_S$ in (b) is the screen length.

**ADVANCED
SCIENCE NEWS**

www.advancedsciencenews.com

**ADVANCED
FUNCTIONAL
MATERIALS**

www.afm-journal.de

imposes on the contact resistance between the electrode and OTS material.[3,32,33] This means the electric field inside the OTS material becomes small when it switches to the ON state. The proposed melting mechanism here can explain that even though the electric field inside the OTS materials decreased sharply after the switching-ON process, the conducting filament can be maintained through the Joule heating effect of holding current. Furthermore, The melting process can also help to explain the failure of endurance[3] in OTS materials, because the tendency for phase separation (as reflected by a stronger ability to form Ge-Ge bonds with increasing temperature, especially in *l*-GeSe, see Figure 1e) and atomic interdiffusion between electrode and OTS material increases with rising temperature.

3. Conclusion

In summary, the present work reveals the temperature-dependent atomic and electronic structures of the typical OTS material GeSe. The increase in temperature leads to significant structural and chemical disorders but surprisingly results in a delocalization of band-tail states at around Fermi level, which originally are localized at room temperature. In particular, the melting of *a*-GeSe would eliminate its band gap, and then increase the concentration of carriers. All of these make the OTS material transform from an insulating state (*a*-GeSe) to a conductive state (*l*-GeSe) after melting. As such, the liquid OTS material can hold the ON state in OTS+PCM devices. Such a picture explains several phenomena in OTS devices, such as the thickness-independent holding voltage and the limited endurance. Possible strategies to optimize OTS devices are suggested. For example, one can reduce the number of element types of OTS materials to suppress melting-induced phase separation, and choose suitable electrodes and buffer layers[17,34] to prevent atomic interdiffusions. Strong glass-forming ability after the melt-quenching process is also an important fingerprint for OTS materials. Therefore, thermal-management engineering will be a critical way to improve performances in OTS+PCM devices. The present work offers a detained atomic/electronic picture of OTS materials for applications in 3D crossbar memory technology.

4. Experimental Section

First-Principles Calculations and Ab Initio Molecular Dynamics: Calculations based on density-functional theory (DFT) were performed using the Vienna ab initio simulation package (VASP).[35–37] Projector augmented-wave (PAW) pseudopotentials with generalized gradient approximation (GGA) exchange-correlation functional developed by Perdew, Burke and Ernzerhof (PBE) were adopted.[37–39] The cutoff energy for plane-wave expansion was 275 eV for property evaluations and 220 eV for molecular dynamics (MD). The k-point grids for integration of the Brillouin zone were Monkhorst−Pack grid of $3 \times 3 \times 3$ for property calculation and $1 \times 1 \times 1$ (Γ point) for MD. The reasonability of the cutoff energy and k-point grids were tested using higher-precision values (see Note S4, Figures S9 and S10, Supporting Information). MD simulations were performed using a time step of 3 fs within a canonical (NVT) ensemble. We use the NVT ensemble here because conducting filaments were usually confined inside OTS materials.[33] The models of GeSe contain 108 Ge and 108 Se atoms. The liquid and amorphous models of GeSe are obtained by the melt-quench method[40] with following steps: 1) the structure is fully diffused for 9 ps at a high temperature of 3000 K; 2) the liquid state was

maintained at 1100, 1300, and 1500 K, respectively for 15 ps; 3) the liquid at 1100 K (around the melting point of crystalline GeSe) is quenched to 300 K with a rate of 15 K ps^{-1}, and then the amorphous phase is maintained at 300 K for 15 ps; 4) a 15-ps MD at 700 K was run starting from the amorphous phase at 300 K. Structural analyses, such as pair correlation function and bond angle distribution, were averaged by the last 3-ps structures (1000 frames) in MD. The cutoff distance for the bonding was 1.3 times the sum of the covalent radii of elements. The partial density of state (PDOS) and crystal orbital Hamilton population (COHP) were analyzed using the LOBSTER code.[41–43]

[1] P. W. Anderson, *Phys. Rev.* **1958**, *109*, 1492.
[2] S. R. Ovshinsky, *J. Non Cryst. Solids* **1970**, *2*, 99.
[3] G. W. Burr, R. S. Shenoy, K. Virwani, P. Narayanan, A. Padilla, B. Kurdi, H. Hwang, *J. Vac. Sci. Technol. B* **2014**, *32*, 040802.
[4] H. K. Henisch, E. A. Fagen, S. R. Ovshinsky, *J. Non Cryst. Solids* **1970**, *4*, 538.
[5] D. Adler, M. S. Shur, M. Silver, S. R. Ovshinsky, *J. Appl. Phys.* **1980**, *51*, 3289.
[6] D. Ielmini, *Phys. Rev. B* **2008**, *78*, 035308.
[7] D. Ielmini, Y. Zhang, *J. Appl. Phys.* **2007**, *102*, 054517.
[8] C. Jacoboni, E. Piccinini, F. Buscemi, A. Cappelli, *Solid State Electron* **2013**, *84*, 90.
[9] S. Jia, H. Li, T. Gotoh, C. Longeaud, B. Zhang, J. Lyu, S. Lv, M. Zhu, Z. Song, Q. Liu, J. Robertson, M. Liu, *Nat. Commun.* **2020**, *11*, 4636.

**ADVANCED
SCIENCE NEWS**

www.advancedsciencenews.com

**ADVANCED
FUNCTIONAL
MATERIALS**

www.afm-journal.de

[10] V. G. Karpov, Y. A. Kryukov, S. D. Savransky, I. V. Karpov, *Appl. Phys. Lett.* **2007**, *90*, 123504.

[11] M. Le Gallo, A. Athmanathan, D. Krebs, A. Sebastian, *J. Appl. Phys.* **2016**, *119*, 025704.

[12] J. Liu, *IEEE T. Electron Dev.* **2017**, *64*, 2207.

[13] P. Noe, A. Verdy, F. d'Acapito, J. B. Dory, M. Bernard, G. Navarro, J. B. Jager, J. Gaudin, J. Y. Raty, *Sci. Adv.* **2020**, *6*, eaay2830.

[14] A. Pirovano, A. L. Lacaita, A. Benvenuti, F. Pellizzer, R. Bez, *IEEE T. Electron Dev.* **2004**, *51*, 452.

[15] G. C. Vezzoli, P. J. Walsh, L. W Doremus, *J. Non Cryst. Solids* **1975**, *18*, 333.

[16] M. Le Gallo, A. Sebastian, *J. Phys. D: Appl. Phys.* **2020**, *53*, 213002.

[17] W.-C. Chien, C.-W. Yeh, R. L. Bruce, H.-Y. Cheng, I. T. Kuo, C.-H. Yang, A. Ray, H. Miyazoe, W. Kim, F. Carta, E.-K. Lai, M. J. BrightSky, H.-L. Lung, *IEEE T. Electron Dev.* **2018**, *65*, 5172.

[18] V. L. Deringer, W. Zhang, M. Lumeij, S. Maintz, M. Wuttig, R. Mazzarello, R. Dronskowski, *Angew. Chem. Int. Ed. Engl.* **2014**, *53*, 10817.

[19] F. Urbach, *Phys. Rev.* **1953**, *92*, 1324.

[20] N.-K. Chen, X.-B. Li, X.-P. Wang, S.-Y. Xie, W. Q. Tian, S. Zhang, H.-B. Sun, *IEEE T. Nanotechnol.* **2018**, *17*, 140.

[21] J. Luckas, S. Kremers, D. Krebs, M. Salinga, M. Wuttig, C. Longeaud, *J. Appl. Phys.* **2011**, *110*, 013719.

[22] M. Rutten, M. Kaes, A. Albert, M. Wuttig, M. Salinga, *Sci. Rep.* **2015**, *5*, 17362.

[23] H. Y. Fan, *Phys. Rev.* **1951**, *82*, 900.

[24] J. F. Justo, F. de Brito Mota, A. Fazzio, *Phys. Rev. B* **2002**, *65*, 073202.

[25] B. Silvi, A. Savin, *Nature* **1994**, *371*, 683.

[26] C. Kittel, *Introduction to Solid State Physics*, Wiley & Sons, Inc., Hoboken, **2005**.

[27] R. W. Haisty, H. Krebs, *J. Non Cryst. Solids* **1969**, *1*, 399.

[28] H. Krebs, P. Fischer, *Discuss. Faraday Soc.* **1970**, *50*, 35.

[29] J. Shen, S. Jia, N. Shi, Q. Ge, T. Gotoh, S. Lv, Q. Liu, R. Dronskowski, S. R. Elliott, Z. Song, M. Zhu, *Science* **2021**, *374*, 1390.

[30] T. Kato, K. Tanaka, *Jpn. J. Appl. Phys.* **2005**, *44*, 7340.

[31] I. Petri, P. S. Salmon, H. E. Fischer, *J. Phys.: Condens. Matter* **1999**, *11*, 7051.

[32] D. Adler, H. K. Henisch, S. N. Mott, *Rev. Mod. Phys.* **1978**, *50*, 209.

[33] W. Czubatyj, S. J. Hudgens, *Electron. Mater. Lett.* **2012**, *8*, 157.

[34] C. W. Yeh, W. C. Chien, R. L. Bruce, H. Y. Cheng, I. T. Kuo, C. H. Yang, A. Ray, H. Miyazoe, W. Kim, F. Carta, E. K. Lai, M. BrightSky, H. L. Lung, in 2018 IEEE Symposium on VLSI Technology **2018**, 205.

[35] G. Kresse, J. Furthmuller, *Comput. Mater. Sci.* **1996**, *6*, 15.

[36] G. Kresse, J. Furthmuller, *Phys. Rev. B* **1996**, *54*, 11169.

[37] G. Kresse, D. Joubert, *Phys. Rev. B* **1999**, *59*, 1758.

[38] P. E. Blochl, *Phys. Rev. B* **1994**, *50*, 17953.

[39] J. P. Perdew, K. Burke, M. Ernzerhof, *Phys. Rev. Lett.* **1996**, *77*, 3865.

[40] J. Hegedus, S. R. Elliott, *Nat. Mater.* **2008**, *7*, 399.

[41] V. L. Deringer, A. L. Tchougreeff, R. Dronskowski, *J. Phys. Chem. A* **2011**, *115*, 5461.

[42] S. Maintz, V. L. Deringer, A. L. Tchougreeff, R. Dronskowski, *J. Comput. Chem.* **2013**, *34*, 2557.

[43] S. Maintz, V. L. Deringer, A. L. Tchougreeff, R. Dronskowski, *J. Comput. Chem.* **2016**, *37*, 1030.